

Frustrated Magnetism, Symmetries and \mathbb{Z}_2 -Equivariant Topology

Shayan Zahedi*

Institut für Theoretische Physik, Universität zu Köln, 50937 Cologne, Germany

13 April 2024

Abstract

A novel lemma in \mathbb{Z}_2 -equivariant homotopy theory is stated, proven and applied to the topological classification of frustrated magnets in the presence of canonical time-reversal symmetry. This lemma generalises a result which had been key to the homotopical derivation of the renowned Bott-Kitaev periodic table for topological insulators and superconductors. We distinguish between three symmetry classes AIII, AIII/BDI, and AIII/CII depending on the existence and type of canonical time-reversal symmetry. For each of these classes, the relevant objects to classify are \mathbb{Z}_2 -equivariant maps into a Stiefel manifold. The topological classification is illustrated through examples of frustrated spin models and is compared to the one of Roychowdhury and Lawler (RL).

Keywords: Classical spin liquids, homotopy theory, topological classification, time-reversal symmetry, rigidity matrix, \mathbb{Z}_2 -equivariance, loop space, Bott-Kitaev periodic table, topological insulators and superconductors, topological invariants, Heisenberg antiferromagnets

1 Introduction

The notion of frustration describes the situation where a spin (or several spins) in a spin model cannot find an orientation to fully minimise all the interaction energies with its neighbouring spins simultaneously (see Figure 1.1(a)). In general, frustration is caused either by competing interactions, as in the Villain model [42], or by the lattice structure as in the triangular, face-centred cubic (fcc) and hexagonal-close-packed (hcp) lattices, with antiferromagnetic nearest neighbour exchange interactions [6, p. 2]. When the geometry of a lattice precludes the simultaneous minimisation of all interactions, one speaks of a geometrically frustrated system [28].

We are interested in studying the topology of zero modes in frustrated systems. A consequence of frustration is an accidental degeneracy of ground states, that is, two different ground states are not generally related by any symmetry operation. Therefore, Hermitian matrices are not of direct use to describe zero modes in frustrated magnets as frustration cannot be attributed to the symmetries of a Hamiltonian. Instead, for each ground state of a frustrated system, one identifies the key object: a continuous linear transformation from the space of spin wave degrees of freedom into the space of ground state constraints, the *rigidity matrix* [31]. Ground state constraints are the conditions that have to be satisfied to put the system under inspection into

*zahedi@thp.uni-koeln.de

one of its ground states. Rigidity matrices are rectangular matrices and their kernels are the spaces of zero modes. They describe the topology of zero modes in frustrated magnets.

For continuous spins, one can estimate the size of ground state degeneracy of frustrated spin models through the *Maxwellian counting argument* [28, 31, 20, p. 8]. The key idea is to reorganise the terms in the spin Hamiltonian into constraints following which the naive degeneracy estimate ν , the *Maxwell counting index*, is obtained. It is the number of ground state degrees of freedom per unit cell and is given as the difference between the total number N of spin wave degrees of freedom per unit cell and the number M of ground state constraints per unit cell, that is, $\nu = N - M$.

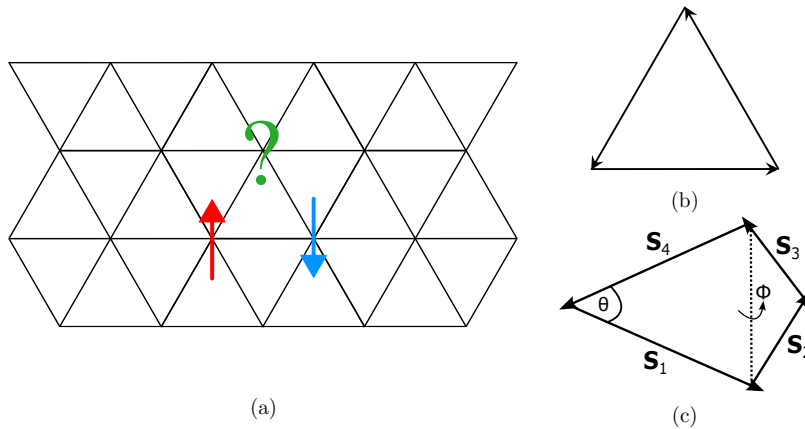


Figure 1.1: On a triangular lattice (a) with antiferromagnetic interactions between nearest neighbours, a configuration in which each spin can be antialigned with all its neighbours is impossible. In other words, the system is frustrated. In each ground state of a cluster of Heisenberg spins, the sum of spins must add up to zero. A cluster of three spins (b) forms a unique structure, whereas a cluster of four spins (c) forms a family of degenerate ground states, parameterised by the structure's two degrees of freedom θ and ϕ .

Maxwell introduced such counting to discuss the stability of mechanical systems of joined rods in 1864 [23]. Chalker and Moessner applied it to frustrated spin systems in 1998 [26], in particular to the pyrochlore (see Figure 2.3) Heisenberg antiferromagnet (HAF) [27]. It can be shown that the number of ground state degrees of freedom of the entire pyrochlore HAF is extensive as it equals the number of tetrahedra [30, 26, 20, p. 9] and one finds $\nu = 2$ for the pyrochlore HAF [20, p. 9] (see Figure 1.1(c)), $\nu = 0$ for the kagome HAF [31] (see Figure 1.1(b)) and $\nu = 1$ for the HAF on a checkerboard lattice [21, 2]. The corresponding constraints in the spin Hamiltonians are that the total spin vanishes in each tetrahedron for the pyrochlore HAF, in each triangle for the kagome HAF, and in each checkerboard for the HAF on the checkerboard lattice, respectively [31].

There is a gap condition for systems described by a rigidity matrix: the number of nonzero singular values is the rank of the rigidity matrix and the introduction of a new zero mode, i.e., a gap closure, means the reduction of this rank. One makes this gap condition more visible by flattening the singular values of rigidity matrices [31]. This flattening of singular values is mathematically realised through a strong deformation retraction. Singular value flattened rigidity matrices take values in complex Stiefel manifolds. The corresponding linearized Hamiltonian, governing the dynamics of spin waves, is given as a bilinear form in terms of the rigidity matrix.

RL [31] topologically classify frustrated systems in the presence of time-reversal symmetry and C_2 rotation symmetry leading to a trivial \mathbb{Z}_2 -action on the Brillouin torus $T^d = \mathbb{R}^d / 2\pi\mathbb{Z}^d$. We develop a homotopical classification of frustrated systems, resulting in the Tables 3.1(a), 3.1(b) and 3.2, by considering momentum-inversion on the Brillouin torus T^d coming from the sole presence of canonical time-reversal symmetry. Depending on the presence and type of canonical time-reversal symmetry, we distinguish between the three symmetry classes AIII, AIII/BDI and AIII/CII (see Table 2.1 for an elaboration on the symmetry labels). We also propose the notion and distinction between “strong” and “weak” topological invariants. Our consideration is mainly based on strong topological invariants by substituting T^d with the d -sphere S^d which reveals sets of homotopy classes beyond those in the Bott-Kitaev periodic table for topological insulators and superconductors [16, 19, 22, 34, 38]. The homotopical classification is performed as a function of the number of ground state degrees of freedom per unit cell ν , the underlying lattice dimension d and depends on the realisation of canonical time-reversal symmetry. In distinction to RL [31], the absence of any further crystalline symmetries is considered.

To achieve such a topological classification of frustrated systems in the presence of canonical time-reversal symmetry, we formulate, prove and apply one of our main results, Lemma 3.1. Lemma 3.1 constitutes a generalisation of a result in \mathbb{Z}_2 -equivariant homotopy theory and establishes an isomorphism between homotopy groups of \mathbb{Z}_2 -equivariant iterated loop spaces and relative homotopy groups of pairs of iterated loop spaces, involving a dimensional shift. More on \mathbb{Z}_2 -equivariant loop spaces is presented in [43].

A weaker variant of Lemma 3.1 was previously formulated only for the loop space of certain symmetric spaces in the context of free-fermion ground states of gapped systems with symmetries [18, Lemma 5.13] and is here generalised through the iteration of the loop space construction applied to arbitrary \mathbb{Z}_2 -spaces. Another weaker variant, for the study of three-dimensional insulators with inversion symmetry, was intuitively stated in [41]. Motivated by [31], we apply Lemma 3.1 to classify the topology of zero modes in frustrated magnets in the presence of canonical time-reversal symmetry. Technically, this lemma always finds applications as long as \mathbb{Z}_2 -equivariance conditions are present, the \mathbb{Z}_2 -action on the Brillouin torus T^d is realised through momentum-inversion [3, 18, 10, 14, 15] and T^d can be replaced by S^d at the expense of losing weak topological invariants.

In recent studies, classical spin liquids are classified based on their energy spectrum [9, 45]. A more detailed development and comprehensive exposition of the classification theory with numerous examples can be found in [44].

This paper is organised as follows: in chapter 2 we introduce the physical framework to describe spin waves of frustrated magnets through a mathematical model and examples. The examples include a classical HAF on a square lattice with anisotropic next-nearest neighbour exchange interactions, the classical $J_1 - J_2$ HAF on a square lattice and the classical pyrochlore HAF. In these examples, rigidity matrices are computed and symmetries are identified.

In chapter 3 we formulate and prove one of the main results, Lemma 3.1. It is applied to obtain a topological classification of zero modes characterised by time-reversal symmetric (i.e. \mathbb{Z}_2 -equivariant) rigidity matrices (see Tables 3.1(a) and 3.1(b)). Furthermore, it is argued that target spaces of rigidity matrices are, after minimal assumptions and an appropriate deformation retraction, complex Stiefel manifolds. The homotopical classification is exemplified through the

examples in chapter 2 and compared to the topological classification of RL [31] and their time-reversal related symmetry considerations.

2 The Physical Framework

The goal of this chapter is to introduce a physical framework in which we describe spin waves, the linearised degrees of freedom in the ground states of a frustrated system, and ground state constraints. The notion of time-reversal symmetry is introduced and three different \mathbb{Z}_2 -equivariance conditions are obtained as a consequence.

Physical examples of calculating rigidity matrices and identifying their symmetries are demonstrated. We consider the classical HAF on a square lattice with anisotropic next-nearest neighbour exchange interactions, the $J_1 - J_2$ HAF on a square lattice and the classical pyrochlore HAF.

2.1 A Mathematical Model

We consider a d -dimensional underlying lattice \mathbb{Z}^d (position space) with minimal distance normalised to 1 and associate to each lattice position a unit cell \mathbb{C}^N with N spin wave degrees of freedom in a frustrated system. In the case of three-component spins having unit magnitude, each spin can be associated with a 2-sphere S^2 and is restricted to a subspace of S^2 in the ground state. Choosing a certain ground state configuration (which amounts to fixing spin axes), each spin's linearised degrees of freedom live in the plane orthogonal to the spin axes, see Figure 2.1.

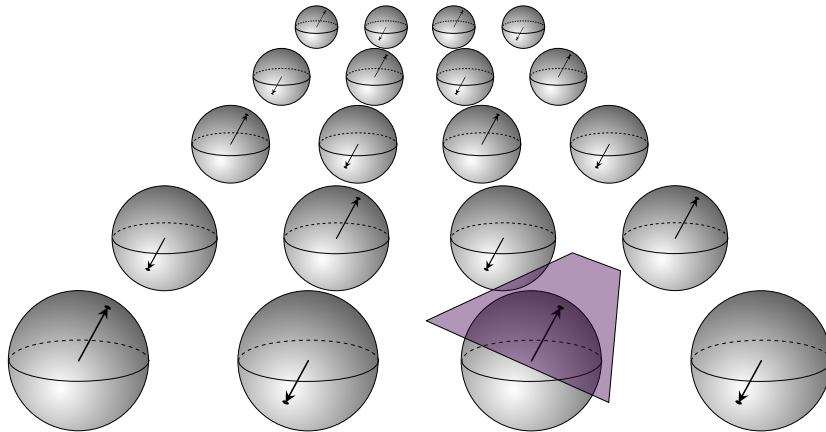


Figure 2.1: A Néel ordered state serves as one of many ground states of the $J_1 - J_2$ HAF on a square lattice [31]. The Néel vector can be chosen arbitrarily, tracing out the whole 2-sphere S^2 (grey), and expanding around any ground state amounts to considering linearised degrees of freedom coming from the planes (purple) orthogonal to the fixed spin axes (schematic illustration).

In analogy to phase space, we assume our number of linearised degrees of freedom to be even. Therefore, the planes perpendicular to the spin axes (being isomorphic to one another)

are modelled by $\mathbb{C}^N \cong \mathbb{R}^{2N}$. The complex Hilbert space containing the spin waves is hence modelled by

$$\mathcal{H}_d^N := \ell^2(\mathbb{Z}^d, \mathbb{C}^N) = \left\{ \varphi: \mathbb{Z}^d \rightarrow \mathbb{C}^N \mid \sum_{i=1}^N \sum_{\mathbf{x} \in \mathbb{Z}^d} |\varphi_i(\mathbf{x})|^2 < \infty \right\} \quad (2.1)$$

with the scalar product

$$\langle \varphi, \psi \rangle_{\mathcal{H}_d^N} := \sum_{\mathbf{x} \in \mathbb{Z}^d} \langle \varphi(\mathbf{x}), \psi(\mathbf{x}) \rangle_{\mathbb{C}^N} \quad (2.2)$$

which serves as a conventional tool for upcoming calculations. The square summability condition on our spin waves is needed to perform a Fourier transformation later.

Although the form of the lattice \mathbb{G} describing the positions of the constraints is model-dependent because it depends, among other things, on the interactions between the spins, we consider $\mathbb{G} = \mathbb{Z}^d$ without loss of generality. The reason is that an isomorphism $\mathbb{G} \cong \mathbb{Z}^d$ is already enough to remain in the framework of the upcoming topological classification. The Hilbert space \mathcal{H}_d^M appropriately models the space of ground state constraints.

We immediately see that $\mathcal{B}_d^N := \{\delta_{\mathbf{x}} e_i \mid \mathbf{x} \in \mathbb{Z}^d \text{ and } 1 \leq i \leq N\}$ constitutes an orthonormal basis for \mathcal{H}_d^N , where

$$\delta_{\mathbf{x}}(\mathbf{y}) := \begin{cases} 1 & \text{for } \mathbf{y} = \mathbf{x}, \\ 0 & \text{otherwise.} \end{cases} \quad (2.3)$$

For every $\mathbf{a} \in \mathbb{Z}^d$, we define translation operators as the unitary operators $t_{\mathbf{a}}: \mathcal{H}_d^N \rightarrow \mathcal{H}_d^N$, $t_{\mathbf{a}}(\delta_{\mathbf{x}} e_i) := \delta_{\mathbf{x}+\mathbf{a}} e_i$, and linear extension. Following [1], time-reversal operators are either real or quaternionic structures, i.e. antiunitary operators $T = UK: \mathcal{H}_d^N \rightarrow \mathcal{H}_d^N$ squaring either to $+\text{Id}_{\mathcal{H}_d^N}$ or to $-\text{Id}_{\mathcal{H}_d^N}$. Here, U is a unitary operator and K is the operation of complex conjugation concerning the basis \mathcal{B}_d^N . Linearised degrees of freedom and ground state constraints assume values in $\mathbb{R}^{2N} \cong \mathbb{C}^N$ and $\mathbb{R}^{2M} \cong \mathbb{C}^M$. These spaces are essentially classical phase spaces. This is the reason for realising time-reversal operators on both spaces \mathcal{H}_d^N and \mathcal{H}_d^M as real or quaternionic structures (having the effect of reversing the sign of the symplectic structure of phase space).

Densely defined linear operators $R: \mathcal{D}(R) \subseteq \mathcal{H}_d^N \rightarrow \mathcal{H}_d^M$ acting as

$$R(\delta_{\mathbf{y}} e_j) = \sum_{i=1}^M \sum_{\mathbf{x} \in \mathbb{Z}^d} \tilde{R}_{ij}(\mathbf{x}, \mathbf{y}) \delta_{\mathbf{x}} e_i, \quad (2.4)$$

are uniquely characterised by their matrix representation $\tilde{R}: \mathbb{Z}^d \times \mathbb{Z}^d \rightarrow \mathbb{C}^{M \times N}$. We specifically classify the cases in which $\tilde{U}(\mathbf{x}, \mathbf{y}) = \delta_{\mathbf{x}}(\mathbf{y}) J$ with J being in its *standard form*¹ [8, 40, 31, 7, Chapter 16]

$$J = \begin{cases} I_N & \text{for } T^2 = +\text{Id}_{\mathcal{H}_d^N}, \\ I_{N/2} \otimes i\sigma_2 & \text{for } T^2 = -\text{Id}_{\mathcal{H}_d^N}. \end{cases} \quad (2.5)$$

Motivated by the examples in chapter 2.2, we will work with translation invariant time-reversal

¹Note that in the case $T^2 = -\text{Id}_{\mathcal{H}_d^N}$ one can show easily that N must be even. The matrix I_N denotes the $N \times N$ identity matrix. The σ_i denote Pauli matrices.

symmetric *rigidity operators* $R: \mathcal{D}(R) \subseteq \mathcal{H}_d^N \rightarrow \mathcal{H}_d^M$. That is, they satisfy $t_a R = R t_a$ ², $t_a \mathcal{D}(R) = \mathcal{D}(R)$, $T_2 R = R T_1$ and $T_1 \mathcal{D}(R) = \mathcal{D}(R)$, or equivalently $\tilde{R}(\mathbf{x} + \mathbf{a}, \mathbf{y} + \mathbf{a}) = \tilde{R}(\mathbf{x}, \mathbf{y})$ and $J_2 \tilde{R}(\mathbf{x}, \mathbf{y}) J_1^\dagger = \tilde{R}(\mathbf{x}, \mathbf{y})$ for all $\mathbf{a}, \mathbf{x}, \mathbf{y} \in \mathbb{Z}^d$ implying that R is uniquely characterised by $r: \mathbb{Z}^d \rightarrow (\mathbb{C}^{M \times N})^{\mathbb{Z}_2}$, $r(\mathbf{x}) := R(\mathbf{x}, \mathbf{0})$. Here, T_1 and T_2 are both either real or quaternionic structures on \mathcal{H}_d^N and \mathcal{H}_d^M respectively and

$$\left(\mathbb{C}^{M \times N}\right)^{\mathbb{Z}_2} \cong \begin{cases} \mathbb{C}^{M \times N} & \text{no time-reversal symmetry,} \\ \mathbb{R}^{M \times N} & \text{for } T_1^2 = +\text{Id}_{\mathcal{H}_d^N} \text{ and } T_2^2 = +\text{Id}_{\mathcal{H}_d^M}, \\ \mathbb{H}^{M/2 \times N/2} & \text{for } T_1^2 = -\text{Id}_{\mathcal{H}_d^N} \text{ and } T_2^2 = -\text{Id}_{\mathcal{H}_d^M}, \end{cases} \quad (2.6)$$

is the \mathbb{Z}_2 -fixed point set concerning the \mathbb{Z}_2 -action $g\Lambda := J_2 \bar{\Lambda} J_1^\dagger$, where $g \in \mathbb{Z}_2$ denotes the nontrivial element.

Through the Fourier transformation $F: \mathcal{H}_d^N \rightarrow L^2(T^d, \mathbb{C}^N) =: \mathcal{K}_d^N$, given by $F(\delta_{\mathbf{x}} e_i) := e_{\mathbf{x}} e_i$ and linear extension, we see that rigidity operators $R' := F R F^\dagger: F\mathcal{D}(R) \subseteq \mathcal{K}_d^N \rightarrow \mathcal{K}_d^M$ act diagonally on momentum space because $R' \tilde{\varphi} = \tilde{r} \tilde{\varphi}$ with

$$\tilde{r}(\mathbf{k}) := \sum_{\mathbf{x} \in \mathbb{Z}^d} r(\mathbf{x}) e^{i\mathbf{k}\mathbf{x}}. \quad (2.7)$$

Here, $e_{\mathbf{x}}(\mathbf{k}) := e^{i\mathbf{k}\mathbf{x}} / (2\pi)^{d/2}$.

That is, R' acts through multiplication by the *rigidity matrix* $\tilde{r}: T^d \rightarrow \mathbb{C}^{M \times N}$. Using the rank-nullity theorem [11, p. 70], one can reexpress the Maxwell counting index in terms of rigidity matrices as $\nu = \text{nullity } \tilde{r} - \text{nullity } \tilde{r}^\dagger$, being a special case of an analytical index [29, p. 453].

The corresponding linearized Hamiltonian governing the spin wave dynamics is $H = R^\dagger R$ [31, 32], i.e., a bilinear form in terms of R . It acts diagonally in momentum space through multiplication by $\tilde{h} = \tilde{r}^\dagger \tilde{r}: T^d \rightarrow \mathbb{C}^{N \times N}$. All zero modes in a frustrated model can be explained in the framework of rigidity operators whose kernel $\ker H = \ker R$ contains the zero modes. Any zero mode $\tilde{\varphi} \in F \ker R$ equivalently satisfies $\tilde{\varphi}(\mathbf{k}) \in \ker \tilde{r}(\mathbf{k})$ for almost all $\mathbf{k} \in T^d$. Therefore, a classification of rigidity matrices directly addresses the question of how frustration can be preserved by perturbations [31].

We are specifically concerned with rigidity operators R whose rigidity matrices \tilde{r} are continuous [31, 32] and \mathbb{Z}_2 -equivariant, distinguishing the following three cases. The symmetry labels in Table 2.1 are borrowed from [33] in the following sense: compared to this classification, RL [31, 33] solely consider BDI and CII in the presence of symmetries.

²We use the same notation for translation operators on both \mathcal{H}_d^N and \mathcal{H}_d^M . Similarly, this is done for the notation of upcoming Fourier transformations.

Label	Time-reversal symmetry	\mathbb{Z}_2 -equivariance of $\tilde{r}: T^d \rightarrow \mathbb{C}^{M \times N}$
AIII	no	trivial \mathbb{Z}_2 -equivariance
AIII/BDI	yes, $T_1^2 = +\text{Id}_{\mathcal{H}_d^N}$, $T_2^2 = +\text{Id}_{\mathcal{H}_d^M}$	$\tilde{r}(-\mathbf{k}) = \overline{\tilde{r}(\mathbf{k})}$
AIII/CII	yes, $T_1^2 = -\text{Id}_{\mathcal{H}_d^N}$, $T_2^2 = -\text{Id}_{\mathcal{H}_d^M}$	$\tilde{r}(-\mathbf{k}) = (I_{M/2} \otimes \sigma_2) \overline{\tilde{r}(\mathbf{k})} (I_{N/2} \otimes \sigma_2)$

Table 2.1: We present the \mathbb{Z}_2 -equivariance conditions on the rigidity matrix $\tilde{r}: T^d \rightarrow \mathbb{C}^{M \times N}$ as a consequence of the existence and type of canonical time-reversal symmetry. An elaboration on the symmetry labels is called for. For any $[\mathbf{k}] \in T^d$, we certainly know $\tilde{r}(\mathbf{k}) \in \mathbb{C}^{M \times N}$ explaining the label AIII in all three cases. In the presence of time-reversal symmetry, we further have $\tilde{r}(\mathbf{k}) \in (\mathbb{C}^{M \times N})^{\mathbb{Z}_2}$ (see equation (2.6)) for time-reversal invariant momenta $[\mathbf{k}] \in (T^d)^{\mathbb{Z}_2}$, leading to the label BDI or to CII depending on the realisation of time-reversal symmetry.

The \mathbb{Z}_2 -action of time-reversal on the Brillouin torus $T^d = \mathbb{R}^d/2\pi\mathbb{Z}^d \cong (I/\partial I)^d$, with $I := [-\pi, \pi]$, is given as $g[\mathbf{k}] = [-\mathbf{k}]$. Time-reversal invariant momenta live in the finitely generated subgroup $(T^d)^{\mathbb{Z}_2} = \langle [\pi e_1], \dots, [\pi e_d] \rangle$ of order $|(T^d)^{\mathbb{Z}_2}| = 2^d$.

2.2 Examples

Altermagnets display a new type of collinear magnetism distinct from ferromagnetism and conventional antiferromagnetism [24, 36, 35]. The altermagnetic Hubbard model [3] inspires us to consider a Néel state of the classical HAF on the square lattice with anisotropic antiferromagnetic next-nearest neighbour exchange interactions depicted in Figure 2.2. The corresponding spin Hamiltonian reads (realising spins as functions $S: \mathbb{Z}^2 \rightarrow S^2$, $\mathbf{x} \mapsto S_{\mathbf{x}}$ and denoting $\mathbf{a}_1 = (1, 0)$ and $\mathbf{a}_2 = (0, 1)$ as primitive vectors)

$$H = J_1 \sum_{\mathbf{x} \in \mathbb{Z}^2} (S_{\mathbf{x}} S_{\mathbf{x}+\mathbf{a}_1} + S_{\mathbf{x}} S_{\mathbf{x}+\mathbf{a}_2}) + J_2 \sum_{\mathbf{x} \in V} (S_{\mathbf{x}} S_{\mathbf{x}+\mathbf{a}_1+\mathbf{a}_2} + S_{\mathbf{x}+\mathbf{a}_1} S_{\mathbf{x}+\mathbf{a}_2}) \quad (2.8a)$$

$$+ J_3 \sum_{\mathbf{x} \in V} (S_{\mathbf{x}} S_{\mathbf{x}+\mathbf{a}_1-\mathbf{a}_2} + S_{\mathbf{x}-\mathbf{a}_2} S_{\mathbf{x}+\mathbf{a}_1})$$

$$= \frac{J_1}{4} \sum_{\mathbf{x} \in V} (S_{\mathbf{x}} + S_{\mathbf{x}+\mathbf{a}_1} + S_{\mathbf{x}+\mathbf{a}_2} + S_{\mathbf{x}+\mathbf{a}_1+\mathbf{a}_2})^2 + \frac{J_1}{4} \sum_{\mathbf{x} \in V} (S_{\mathbf{x}} + S_{\mathbf{x}+\mathbf{a}_1} + S_{\mathbf{x}-\mathbf{a}_2} + S_{\mathbf{x}+\mathbf{a}_1-\mathbf{a}_2})^2$$

$$+ \frac{J_1}{2} \left| \frac{J_2}{J_1} - \frac{1}{2} \right| \sum_{\mathbf{x} \in V} \left[(S_{\mathbf{x}+\mathbf{a}_1} \pm S_{\mathbf{x}+\mathbf{a}_2})^2 + (S_{\mathbf{x}} \pm S_{\mathbf{x}+\mathbf{a}_1+\mathbf{a}_2})^2 \right] \quad (2.8b)$$

$$+ \frac{J_1}{2} \left| \frac{J_3}{J_1} - \frac{1}{2} \right| \sum_{\mathbf{x} \in V} \left[(S_{\mathbf{x}+\mathbf{a}_1} \pm S_{\mathbf{x}-\mathbf{a}_2})^2 + (S_{\mathbf{x}} \pm S_{\mathbf{x}+\mathbf{a}_1-\mathbf{a}_2})^2 \right] + \text{const.}$$

with $V := \mathbb{Z}(\mathbf{a}_1 + \mathbf{a}_2) \oplus \mathbb{Z}(\mathbf{a}_1 - \mathbf{a}_2)$ denoting the lattice of the magnetic unit cells. In equation (2.8b), the sign \pm is used in the case $J_1 \leq 2J_i$ for $i \in \{2, 3\}$. The magnetic unit cell consists of two 0-cells, four 1-cells and two 2-cells (being doubled in size in comparison to the nuclear unit cell which is a square plaquette).

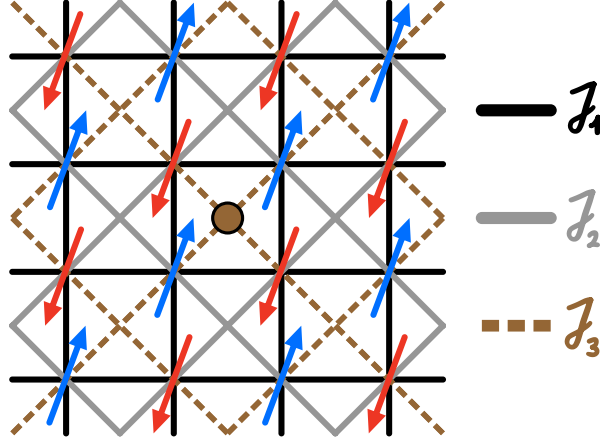


Figure 2.2: The Néel state of the HAF on a square lattice with anisotropic next-nearest neighbour exchange interactions represents a ground state. It is symmetric under a global spin flip followed by a $\pi/2$ rotation around the brown dot of the brown dual square lattice. The nearest neighbour exchange interaction J_1 and next-nearest neighbour exchange interactions J_2 and J_3 are also illustrated.

In the case of $J_1 = 2J_i$ for both $i = 2, 3$, the spin Hamiltonian becomes

$$H = \frac{J_1}{4} \sum_{\mathbf{x} \in \mathbb{Z}^2} (S_{\mathbf{x}} + S_{\mathbf{x}+\mathbf{a}_1} + S_{\mathbf{x}+\mathbf{a}_1} + S_{\mathbf{x}+\mathbf{a}_1+\mathbf{a}_2})^2 + \text{const.} \quad (2.9)$$

and the magnetic unit cell coincides with the nuclear unit cell. Ground states are therefore obtained for $S_{\mathbf{x}} + S_{\mathbf{x}+\mathbf{a}_1} + S_{\mathbf{x}+\mathbf{a}_1} + S_{\mathbf{x}+\mathbf{a}_1+\mathbf{a}_2} = 0$ for all $\mathbf{x} \in \mathbb{Z}^2$. Parameterising the spins via $(p, q) \mapsto (\cos(q)\sqrt{1-p^2}, \sin(q)\sqrt{1-p^2}, p)$ and linearising the ground state constraints along the positive x -axis in the Néel ordered state depicted in Figure 2.2, we obtain the rigidity matrix in momentum space (compare with [31])

$$\tilde{r}(\mathbf{k}) = \begin{pmatrix} 1 - e^{ik_x} - e^{ik_y} + e^{i(k_x+k_y)} & 0 \\ 0 & 1 + e^{ik_x} + e^{ik_y} + e^{i(k_x+k_y)} \end{pmatrix}. \quad (2.10)$$

This rigidity matrix is of symmetry class AIII/BDI (see Table 2.1) and exhibits the Maxwell counting index $\nu = 0$, see Table 3.1(a) (derived by employing the algorithm in equation (A.1)).

Now, in the case $J_1 > 2J_i$ for both $i \in \{2, 3\}$ and $J_2 \neq J_3$, we obtain the ground state constraints $S_{\mathbf{x}} + S_{\mathbf{x}+\mathbf{a}_1} + S_{\mathbf{x}+\mathbf{a}_2} + S_{\mathbf{x}+\mathbf{a}_1+\mathbf{a}_2} = 0$, $S_{\mathbf{x}} + S_{\mathbf{x}+\mathbf{a}_1} + S_{\mathbf{x}-\mathbf{a}_2} + S_{\mathbf{x}+\mathbf{a}_1-\mathbf{a}_2} = 0$, $S_{\mathbf{x}+\mathbf{a}_1} - S_{\mathbf{x}+\mathbf{a}_2} = 0$, $S_{\mathbf{x}} - S_{\mathbf{x}+\mathbf{a}_1+\mathbf{a}_2} = 0$,

$S_{\mathbf{x}+\mathbf{a}_1} - S_{\mathbf{x}-\mathbf{a}_2} = 0$ and $S_{\mathbf{x}} - S_{\mathbf{x}+\mathbf{a}_1-\mathbf{a}_2} = 0$ for all $\mathbf{x} \in V$ and the rigidity matrix reads

$$\tilde{r}(\mathbf{k}) = \begin{pmatrix} 1+e^{ik_x} & -1-e^{-ik_y} & 0 & 0 \\ 1+e^{ik_y} & -1-e^{-ik_x} & 0 & 0 \\ 0 & e^{-ik_y}-1 & 0 & 0 \\ 1-e^{ik_x} & 0 & 0 & 0 \\ 0 & 1-e^{-ik_x} & 0 & 0 \\ e^{ik_y}-1 & 0 & 0 & 0 \\ 0 & 0 & 1+e^{ik_x} & 1+e^{-ik_y} \\ 0 & 0 & 1+e^{ik_y} & 1+e^{-ik_x} \\ 0 & 0 & 0 & 1-e^{-ik_y} \\ 0 & 0 & 1-e^{ik_x} & 0 \\ 0 & 0 & 0 & e^{-ik_x}-1 \\ 0 & 0 & e^{ik_y}-1 & 0 \end{pmatrix} \quad (2.11)$$

being once again of symmetry class AIII/BDI and displaying two submatrices with individual Maxwell counting index $\nu = 4$, see Table 3.1(a). Squaring the $\pi/2$ -rotation symmetry, we find the following additional \mathbb{Z}_2 -equivariance condition $\tilde{r}(-\mathbf{k}) = [((-\sigma_1) \oplus (\sigma_1 \otimes \sigma_1)) \oplus (\sigma_1 \oplus (-\sigma_1 \otimes \sigma_1))] \tilde{r}(\mathbf{k}) [\sigma_1 \oplus \sigma_1]$.

Another example is the classical pyrochlore HAF.

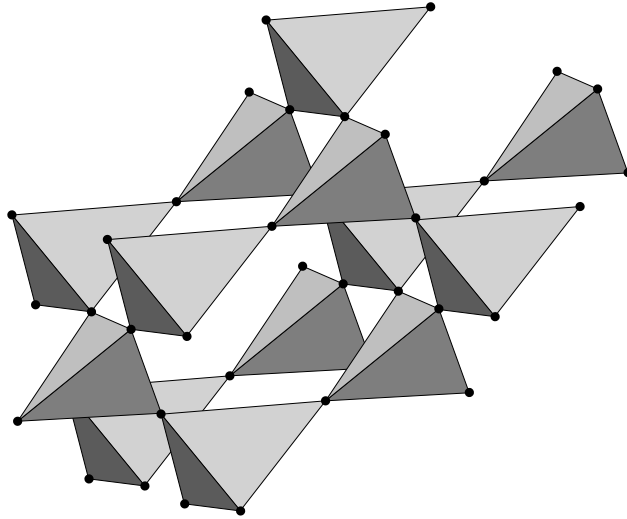


Figure 2.3: The pyrochlore lattice is a network of vertex-sharing tetrahedra.

There are two types of tetrahedra in the pyrochlore lattice, both of which are depicted in Figure 2.4(a). The unit cell of the pyrochlore lattice consists of four 0-cells (indicated by the four blue spin axes in Figure 2.4(a)), twelve 1-cells (all the links between the vertices of the corner-sharing tetrahedra in Figure 2.4(a)), eight 2-cells (all the faces of the corner-sharing tetrahedra in Figure 2.4(a)) and three 3-cells (the two corner-sharing tetrahedra in Figure 2.4(a) and a neighbouring volume).

Orienting the entire pyrochlore lattice along the [111] direction as depicted in Figure 2.4(b), one observes that the pyrochlore lattice consists of alternating kagome and triangular layers stacked on top of each other [39, 20, p. 179]. The lattice describing the positions of the unit

cells for the pyrochlore lattice is, therefore, $\mathbb{P} = \mathbb{Z}\mathbf{a}_1 \oplus \mathbb{Z}\mathbf{a}_2 \oplus \mathbb{Z}\mathbf{a}_3 \subseteq \mathbb{R}^3$ with $\mathbf{a}_1 = (1, 0, 0)$, $\mathbf{a}_2 = (1/2, \sqrt{3}/2, 0)$ and $\mathbf{a}_3 := (3/8, \sqrt{3}/8, \sqrt{13}/4)$. One of the points belonging to this lattice is the corner-sharing point in Figure 2.4(a).

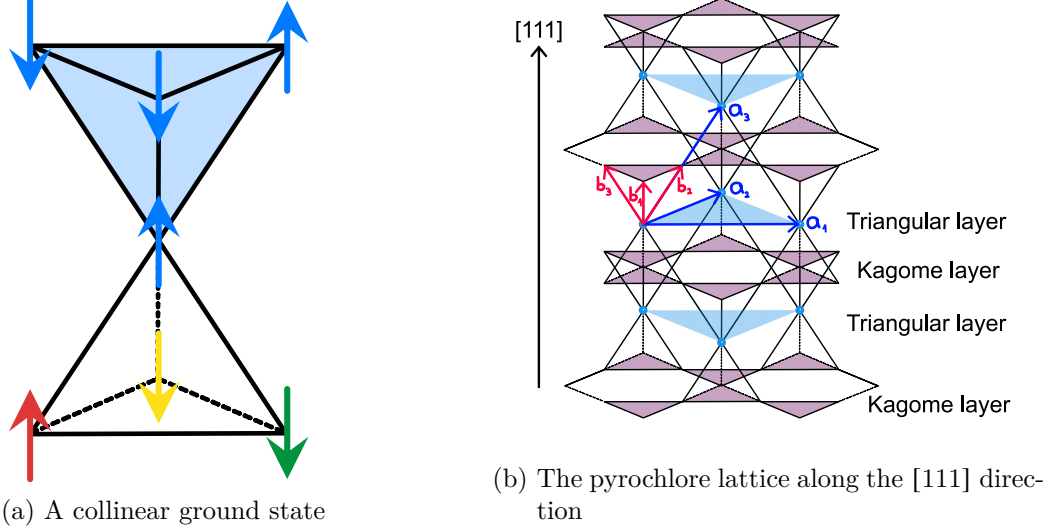


Figure 2.4: A collinear ground state configuration for the pyrochlore HAF is depicted in (a). The spins sitting on the vertices of the blue tetrahedron belong to the same unit cell whereas the yellow, red and green spins belong to neighbouring unit cells respectively. (b) The pyrochlore lattice is an alternating stacking of kagome (purple) and triangular (blue) layers along the [111], body diagonal, direction. The primitive vectors \mathbf{a}_1 , \mathbf{a}_2 and \mathbf{a}_3 span the lattice for the unit cells and the internal vectors $\mathbf{b}_1 := (\mathbf{a}_3 - \mathbf{a}_2)/2$, $\mathbf{b}_2 := \mathbf{a}_3/2$ and $\mathbf{b}_3 := (\mathbf{a}_3 - \mathbf{a}_1)/2$ describe the positions of spins on the kagome layers.

The spin Hamiltonian reads ($J > 0$)

$$\begin{aligned}
H &= J \sum_{\mathbf{x} \in \mathbb{P}} \left[S_{\mathbf{x}} S_{\mathbf{x}+\mathbf{b}_1} + S_{\mathbf{x}} S_{\mathbf{x}+\mathbf{b}_2} + S_{\mathbf{x}} S_{\mathbf{x}+\mathbf{b}_3} + S_{\mathbf{x}+\mathbf{b}_1} S_{\mathbf{x}+\mathbf{b}_2} + S_{\mathbf{x}+\mathbf{b}_2} S_{\mathbf{x}+\mathbf{b}_3} + S_{\mathbf{x}+\mathbf{b}_3} S_{\mathbf{x}+\mathbf{b}_1} \right. \\
&\quad \left. + S_{\mathbf{x}} S_{\mathbf{x}-\mathbf{b}_1} + S_{\mathbf{x}} S_{\mathbf{x}-\mathbf{b}_2} + S_{\mathbf{x}} S_{\mathbf{x}-\mathbf{b}_3} + S_{\mathbf{x}-\mathbf{b}_1} S_{\mathbf{x}-\mathbf{b}_2} + S_{\mathbf{x}-\mathbf{b}_2} S_{\mathbf{x}-\mathbf{b}_3} + S_{\mathbf{x}-\mathbf{b}_3} S_{\mathbf{x}-\mathbf{b}_1} \right] \quad (2.12) \\
&= \frac{J}{2} \sum_{\mathbf{x} \in \mathbb{P}} [L_{1,\mathbf{x}}^2 + L_{2,\mathbf{x}}^2] + \text{const.}
\end{aligned}$$

with $L_{1,\mathbf{x}} := S_{\mathbf{x}} + S_{\mathbf{x}+\mathbf{b}_1} + S_{\mathbf{x}+\mathbf{b}_2} + S_{\mathbf{x}+\mathbf{b}_3}$ and $L_{2,\mathbf{x}} := S_{\mathbf{x}} + S_{\mathbf{x}-\mathbf{b}_1} + S_{\mathbf{x}-\mathbf{b}_2} + S_{\mathbf{x}-\mathbf{b}_3}$ for all $\mathbf{x} \in \mathbb{P}$. Ground states of the pyrochlore HAF are obtained for $L_{2,\mathbf{x}} = 0 = L_{1,\mathbf{x}}$ for all $\mathbf{x} \in \mathbb{P}$. The simplex lattice (describing the positions of the constraints) is a diamond lattice [33]. Considering the collinear ground state [26, 20, pp. 5, 8] of the pyrochlore HAF and, without loss of generality, the direction of the collinear order along the positive x -axis, we obtain the rigidity matrix

$$\tilde{r}(\mathbf{k}) = \begin{pmatrix} 1 & -1 & 1 & -1 & 0 & 0 & 0 & 0 \\ 1 & -e^{i(k_2-k_3)} & e^{-ik_3} & -e^{i(k_1-k_3)} & 0 & 0 & 0 & 0 \\ 0 & 0 & 0 & 0 & 1 & 1 & 1 & 1 \\ 0 & 0 & 0 & 0 & 1 & e^{i(k_2-k_3)} & e^{-ik_3} & e^{i(k_1-k_3)} \end{pmatrix}. \quad (2.13)$$

It is of symmetry class AIII/BDI (see Table 2.1). Here, the rigidity matrix \tilde{r} consists of two

independent blocks representing $\nu = 2$ systems, see Table 3.1(a).

3 The Topological Classification

The examples in chapter 2.2 motivate us to define the space of rigidity matrices R_{dM}^N as the subspace of the space of continuous base point preserving \mathbb{Z}_2 -equivariant maps $\text{Map}_*(T^d, \mathbb{C}^{M \times N})^{\mathbb{Z}_2}$ with the following additional properties. The elements of R_{dM}^N have maximum rank everywhere and are such that if all positive singular values are replaced by 1, another element of $\text{Map}_*(T^d, \mathbb{C}^{M \times N})^{\mathbb{Z}_2}$ is generated. These properties are reflected by the examples in chapter 2.2. Rank-constancy and maximality implement the assumption that the ground state constraints are linearly independent. A topological classification for the general case of fluctuating ranks can be reduced to the constant-and-maximum-rank case³. The base point condition on rigidity matrices is merely a matter of choosing bases in \mathbb{C}^N and \mathbb{C}^M , respectively, at a specific momentum.

It is clear that $\text{Map}_*(T^d, V_n(\mathbb{C}^m))^{\mathbb{Z}_2}$ is homeomorphic to a strong deformation retract of R_{dM}^N , where

$$V_n(\mathbb{C}^m) = \{A \in \mathbb{C}^{m \times n} \mid A^\dagger A = I_n\} \cong \text{U}(m)/\text{U}(m-n) \quad (3.1)$$

denotes the complex Stiefel manifold, $m := \max(M, N)$ and $n := \min(M, N)$. A strong deformation retraction is given by linearly interpolating between the positive singular values of the elements of R_{dM}^N and 1, that is, by *flattening* the singular values in the language of [31]. The \mathbb{Z}_2 -action on $V_n(\mathbb{C}^m)$ is precisely the one described in Table 2.1. Now, modding out \mathbb{Z}_2 -homotopy, one is left with the set of homotopy classes $[T^d, V_n(\mathbb{C}^m)]_*^{\mathbb{Z}_2}$ of base point preserving and \mathbb{Z}_2 -equivariant maps $T^d \rightarrow V_n(\mathbb{C}^m)$ containing strong and weak topological invariants. These sets of homotopy classes classify zero modes in frustrated systems in the presence or absence of canonical time-reversal symmetry.

In the following, the cube $I^d = [-\pi, \pi]^d$ is viewed as a \mathbb{Z}_2 -space through the nontrivial action $g\mathbf{k} := -\mathbf{k}$ and the iterated loop space $\Omega^d X$ of the based \mathbb{Z}_2 -space (X, x_0) denotes the space of all maps $I^d \rightarrow X$ which send ∂I^d to the base point $x_0 \in X^{\mathbb{Z}_2}$. The action of \mathbb{Z}_2 on $\Omega^d X$ is considered to be $(g, f) \mapsto (\mathbf{k} \mapsto gf(-\mathbf{k}))$. Replacing the domain T^d (periodic case) with the d -sphere $S^d \cong I^d/\partial I^d$ (free case), we obtain a topological classification by strong topological invariants at the expense of losing weak topological invariants [33, 17, 34, 37]. Strong and weak topological invariants coincide in dimension $d = 1$ because $T^1 = S^1$. In the following, we are interested in calculating

$$[S^d, V_n(\mathbb{C}^m)]_*^{\mathbb{Z}_2} \cong \left[(I^d, \partial I^d), (V_n(\mathbb{C}^m), E) \right]_{\mathbb{Z}_2} \cong \pi_0 \left(\left(\Omega^d V_n(\mathbb{C}^m) \right)^{\mathbb{Z}_2} \right) \quad (3.2)$$

with $E := (e_1 \cdots e_n)$ denoting the canonical n -frame.

To unlock a deduction of our sought-after homotopical classification of zero modes in frustrated systems, we formulate one of the main results of this paper. Namely, Lemma 3.1 establishes an isomorphism between the homotopy groups of \mathbb{Z}_2 -equivariant iterated loop spaces and

³Indeed, after performing the flattening technique of singular values for the general case, the target spaces of rigidity matrices become unions of Stiefel manifolds and upon choosing a base point, one selects a single Stiefel manifold.

relative homotopy groups of pairs of iterated loop spaces, involving a dimensional shift. This Lemma 3.1 is of vital importance because strong topological invariants are contained in sets of path components (constituting the “zeroth homotopy groups”) of \mathbb{Z}_2 -equivariant iterated loop spaces of complex Stiefel manifolds. More on \mathbb{Z}_2 -equivariant loop spaces can be found in [43].

The following Lemma 3.1 generalises a result that is crucial for the topological classification of free-fermion ground states of gapped systems with symmetries [18, Lemma 5.13] from the loop space of certain symmetric spaces to the iteration of the loop space construction for arbitrary \mathbb{Z}_2 -spaces. Another special case was previously intuitively stated in [41] for the study of three-dimensional insulators with inversion symmetry and is now generalised to any dimension of the underlying lattice. The chosen base points for the left and right-hand side of equation (3.3) are the constant maps to x_0 ⁴. From a purely mathematical point of view, the following lemma should be compared to the simple and familiar statement $\pi_D(\Omega^{d+1}X) \cong \pi_{D+d+1}(X)$ [4, p. 123].

Lemma 3.1. *Let X be a \mathbb{Z}_2 -space, $x_0 \in X$ a \mathbb{Z}_2 -fixed point and $D, d \geq 0$. Then, there is an isomorphism*

$$\pi_D\left(\left(\Omega^{d+1}X\right)^{\mathbb{Z}_2}\right) \cong \pi_{D+1}\left(\Omega^d X, \left(\Omega^d X\right)^{\mathbb{Z}_2}\right). \quad (3.3)$$

Proof. For $D \geq 1$, we set $T := I^D \times [0, \pi]$ and $J_T := \partial I^D \times [0, \pi] \cup I^D \times \{\pi\}$. We set $T = [0, \pi]$ and $J_T = \{\pi\}$ in the case $D = 0$. We use the homeomorphism of triples $(T, \partial T, J_T) \rightarrow (I^{D+1}, \partial I^{D+1}, J^D)$, $(\mathbf{k}, p) \mapsto (\mathbf{k}, 2p - \pi)$ to induce the isomorphism

$$K_{D+1}^d := \left[(T, \partial T, J_T), \left(\Omega^d X, \left(\Omega^d X \right)^{\mathbb{Z}_2}, c_{x_0} \right) \right] \cong \pi_{D+1} \left(\Omega^d X, \left(\Omega^d X \right)^{\mathbb{Z}_2} \right). \quad (3.4)$$

The base point c_{x_0} denotes the constant map to x_0 . Now let $[f] \in \pi_D\left(\left(\Omega^{d+1}X\right)^{\mathbb{Z}_2}\right)$. One easily defines the map⁵

$$\tilde{f}: (T, \partial T, J_T) \rightarrow \left(\Omega^d X, \left(\Omega^d X \right)^{\mathbb{Z}_2}, c_{x_0} \right) \text{ by } \tilde{f}(\mathbf{k}, p) := f(\mathbf{k})(p, -) \quad (3.5)$$

which represents the homotopy class $[\tilde{f}] \in K_{D+1}^d$. This induces the map

$$\eta: \pi_D\left(\left(\Omega^{d+1}X\right)^{\mathbb{Z}_2}\right) \rightarrow K_{D+1}^d \text{ defined by } \eta[f] := [\tilde{f}]. \quad (3.6)$$

The map η is well defined because for $[f] = [g] \in \pi_D\left(\left(\Omega^{d+1}X\right)^{\mathbb{Z}_2}\right)$, there is a homotopy $H: (I^D \times [0, 1], \partial I^D \times [0, 1]) \rightarrow \left(\left(\Omega^{d+1}X\right)^{\mathbb{Z}_2}, c_{x_0}\right)$ from $H_0 = f$ to $H_1 = g$. The homotopy H gives rise to the homotopy $\tilde{H}: (T \times [0, 1], \partial T \times [0, 1], J_T \times [0, 1]) \rightarrow \left(\Omega^d X, \left(\Omega^d X\right)^{\mathbb{Z}_2}, c_{x_0}\right)$ defined by $\tilde{H}_t(\mathbf{k}, p) := H_t(\mathbf{k})(p, -)$ from $\tilde{H}_0 = \tilde{f}$ to $\tilde{H}_1 = \tilde{g}$ implying $\eta[f] = \eta[g]$.

The inverse map

$$\eta^{-1}: K_{D+1}^d \rightarrow \pi_D\left(\left(\Omega^{d+1}X\right)^{\mathbb{Z}_2}\right) \text{ reads } \eta^{-1}[h] = [h'] \quad (3.7)$$

⁴We usually suppress the base point in the notation if the context makes the choice of base point clear.

⁵Standard verifications show that \tilde{f} is indeed such a map of triples.

in which $h': (I^D, \partial I^D) \rightarrow ((\Omega^{d+1}X)^{\mathbb{Z}_2}, c_{x_0})$ is the map

$$h'(\mathbf{k})(p, \mathbf{q}) := \begin{cases} gh(\mathbf{k}, -p)(-\mathbf{q}) & \text{for } p \in [-\pi, 0], \\ h(\mathbf{k}, p)(\mathbf{q}) & \text{for } p \in [0, \pi]. \end{cases} \quad (3.8)$$

Furthermore, η^{-1} is well defined because for $[h] = [k] \in K_{D+1}^d$ there exists a homotopy $F: (T \times [0, 1], \partial T \times [0, 1], J_T \times [0, 1]) \rightarrow (\Omega^d X, (\Omega^d X)^{\mathbb{Z}_2}, c_{x_0})$ from $F_0 = h$ to $F_1 = k$. The map $G: (I^D, \partial I^D) \rightarrow ((\Omega^{d+1}X)^{\mathbb{Z}_2}, c_{x_0})$ defined by $G_t := (F_t)'$ is a homotopy from $G_0 = h'$ to $G_1 = k'$ and therefore, indeed, $\eta^{-1}[h] = \eta^{-1}[k]$. Standard verifications show that $\eta^{-1}\eta = \text{Id}_{\pi_D((\Omega^{d+1}X)^{\mathbb{Z}_2})}$ and $\eta\eta^{-1} = \text{Id}_{K_{D+1}^d}$.

As for now, we have proven that η is a bijection for all $D \geq 0$. Now consider the case $D \geq 1$ and let $[f], [g] \in \pi_D((\Omega^{d+1}X)^{\mathbb{Z}_2})$. It is clear that $\widetilde{f+g} = \widetilde{f} + \widetilde{g}$ ⁶ which implies $\eta([f] + [g]) = \eta[\widetilde{f+g}] = \eta[\widetilde{f} + \widetilde{g}] = \eta[\widetilde{f}] + \eta[\widetilde{g}] = \eta[f] + \eta[g]$ and shows that η is a homomorphism. \square

Applying Lemma 3.1 to the special case $d = 0$, immediately provides

Corollary 3.2. *Let X be a \mathbb{Z}_2 -space, $x_0 \in X$ a \mathbb{Z}_2 -fixed point and $D \geq 0$. There is an isomorphism*

$$\pi_D((\Omega X)^{\mathbb{Z}_2}) \cong \pi_{D+1}(X, X^{\mathbb{Z}_2}) \quad (3.10)$$

\square

Through the algorithm in equation (A.1), one can show inductively

$$\left[(I^d, \partial I^d), (V_{m-|\nu|}(\mathbb{C}^m), E) \right]_{\mathbb{Z}_2} = 0^7 \text{ for all } |\nu| \geq \lceil d/2 \rceil \quad (3.11)$$

in the presence of canonical time-reversal symmetry. In particular, for symmetry class AIII/BDI, we find

$$\left[(I^d, \partial I^d), (S^1, 1) \right]_{\mathbb{Z}_2} \cong \mathbb{Z} \text{ for all } d \geq 1. \quad (3.12)$$

Furthermore, the following Table 3.1 summarises the sets of homotopy classes $\left[(I^d, \partial I^d), (V_{m-|\nu|}(\mathbb{C}^m), E) \right]_{\mathbb{Z}_2}$ containing strong topological invariants in the presence of canonical time-reversal symmetry up to the Brillouin torus dimension $d = 3$.

⁶The operation $+$ on the left-hand side is the standard concatenation of maps

$$(f+g)(\mathbf{k}) := \begin{cases} f(2k_1 + \pi, k_2, \dots, k_D) & \text{for } k_1 \in [-\pi, 0], \\ g(2k_1 - \pi, k_2, \dots, k_D) & \text{for } k_1 \in [0, \pi], \end{cases} \quad (3.9)$$

which descends to the level of homotopy classes delivering a group structure (similarly for the right-hand side).

⁷ $\nu = N - M$

$ \nu $	d			
	1	2	3	
			$m = 1$	$m \geq 2$
0	\mathbb{Z}	\mathbb{Z}	\mathbb{Z}	★
1	0	0		★
≥ 2	0	0		0

(a) Symmetry class AIII/BDI

$ \nu $	d		
	1	2	3
	0	\mathbb{Z}	\mathbb{Z}
≥ 2	0	0	0

(b) Symmetry class AIII/CII

Table 3.1: We display sets of homotopy classes $[(I^d, \partial I^d), (V_{m-|\nu|}(\mathbb{C}^m), E)]_{\mathbb{Z}_2}$ in the presence of canonical time-reversal symmetry realised by (a) real structures or by (b) quaternionic structures. The elements containing a ★ mean yet-to-be-evaluated sets of homotopy classes and indicate the emergence of an unstable regime for all $|\nu| < [d/2]$.

The topological classification in the presence of time-reversal symmetry for higher dimensions $d \geq 4$ of the underlying lattice becomes more complicated compared to the lower dimensional cases. The reason is that for each dimension $d+1$ we require the results from the previous dimension d to make progress (see the algorithm in equation (A.1)).

In the absence of time-reversal symmetry, one classifies through the higher homotopy groups of complex Stiefel manifolds $\pi_d(V_{m-|\nu|}(\mathbb{C}^m))$. These homotopy groups are displayed in Table 3.2 up until dimension $d = 6$ and $|\nu| = 3$ for which the first trivial row appears.

$ \nu $	Dimension d									
	1	2	3	4		5		6		
			$m \geq 2$	$m = 2$	$m \geq 3$	$m = 2$	$m \geq 3$	$m = 2$	$m = 3$	$m \geq 4$
0	\mathbb{Z}	0	\mathbb{Z}	\mathbb{Z}_2	0	\mathbb{Z}_2	\mathbb{Z}	\mathbb{Z}_{12}	\mathbb{Z}_6	0
1	0	0	\mathbb{Z}	\mathbb{Z}_2	0	\mathbb{Z}_2	\mathbb{Z}	\mathbb{Z}_{12}	\mathbb{Z}_6	0
2	0	0	0		0		\mathbb{Z}		\mathbb{Z}_2	\mathbb{Z}_2
≥ 3	0	0	0		0		0			0

Table 3.2: The topological classification for symmetry class AIII is realised by the homotopy groups of complex Stiefel manifolds. The case $\pi_d(U(1)) = \pi_d(S^1) = 0$ for all $d \geq 2$ is omitted in this table from $d = 3$. The entries of the table are taken from [4, p. 148, 12, 25, 13, p. 339].

For the HAF on the square lattice with anisotropic next-nearest neighbour exchange interactions (see Figure 2.2) we investigated the cases $J_1 = 2J_i$ for both $i = 2, 3$ and $J_1 > 2J_i$ for both $i = 2, 3$. In the former, we obtained a rigidity matrix of symmetry class AIII/BDI exhibiting a Maxwell counting index of $\nu = 0$. In the latter, we derived a rigidity matrix composed of two subsystems of symmetry class AIII/BDI exhibiting the Maxwell counting index $\nu = 4$. The former therefore indicates the protection of zero modes by a \mathbb{Z} topology and the latter indicates a trivial topology associated with the Néel state in Figure 2.2 (see Table 3.1(a)). Since the rigidity matrix for the pyrochlore HAF in equation (2.13) consists of two blocks representing systems of symmetry class AIII/BDI with $\nu = 2$, it indicates a trivial topology by Table 3.1(a).

Generally, in the limiting case of $J_2 = J_3$, equation (2.8) becomes the spin Hamiltonian for the $J_1 - J_2$ HAF on a square lattice. In the Néel state, at the critical point (being a highly frustrated point and marking the transition point between the Néel ordered state and the frustrated state)

and in the frustrated state (whose degree of frustration is less than at the critical point) one finds $|\nu| = 2$, $\nu = 0$ and $|\nu| = 1$, respectively [31]. Hence, by Table 3.1(a), the zero modes are protected by a \mathbb{Z} topology at the critical point and the topology is trivial for the Néel state and the frustrated regime.

This topological classification is quite different from the topological classification of RL [31]. In addition to time-reversal symmetry, RL consider the presence of a C_2 rotation symmetry. Therefore, they argue that a \mathbb{Z}_2 invariant would protect the zero modes at the critical point, the unfrustrated Néel state would not be topology protected and that a \mathbb{Z} invariant would protect the frustrated state.

To be more precise, the announced symmetry considerations of RL [31] are time-reversal symmetries. However, their examples hint towards the existence of an additional C_2 rotation symmetry which has a similar effect on momenta in the Brillouin torus T^d as canonical time-reversal symmetry does, namely $[\mathbf{k}] \mapsto [-\mathbf{k}]$. These compositions of symmetries lead to the \mathbb{Z}_2 -invariance conditions $\tilde{r}(-\mathbf{k}) = \overline{\tilde{r}(\mathbf{k})} = \tilde{r}(\mathbf{k})$ (in the presence of time-reversal symmetry by real structures with an additional C_2 -symmetry) and $\tilde{r}(-\mathbf{k}) = (I_{M/2} \otimes \sigma_2) \overline{\tilde{r}(\mathbf{k})} (I_{N/2} \otimes \sigma_2) = \tilde{r}(\mathbf{k})$ (in the presence of time-reversal symmetry by quaternionic structures with an additional C_2 -symmetry). That is, the fixed point condition $g\tilde{r}(\mathbf{k}) = \tilde{r}(\mathbf{k})$ is satisfied for all momenta $[\mathbf{k}] \in T^d$. This is the reason why RL classify the topology of zero modes in frustrated systems with

$$\pi_0 \left(\Omega^d V_n(\mathbb{C}^m)^{\mathbb{Z}_2} \right) \cong \begin{cases} \pi_d(V_n(\mathbb{C}^m)) & \text{no symmetries,} \\ \pi_d(V_n(\mathbb{R}^m)) & \text{for } T_i^2 = +\text{Id and } C_2\text{-symmetry,} \\ \pi_d(V_{n/2}(\mathbb{H}^{m/2})) & \text{for } T_i^2 = -\text{Id and } C_2\text{-symmetry,} \end{cases} \quad (3.13)$$

i.e., the homotopy groups of complex, real and quaternionic Stiefel manifolds. We classify the topology with sets of path components of \mathbb{Z}_2 -equivariant iterated loop spaces of complex Stiefel manifolds

$$\pi_0 \left(\left(\Omega^d V_n(\mathbb{C}^m) \right)^{\mathbb{Z}_2} \right) \cong \pi_1 \left(\Omega^{d-1} V_n(\mathbb{C}^m), \left(\Omega^{d-1} V_n(\mathbb{C}^m) \right)^{\mathbb{Z}_2} \right). \quad (3.14)$$

Considering the \mathbb{Z}_2 -equivariance conditions portrayed in Table 2.1, the fixed point condition is in particular satisfied for all 2^d time-reversal invariant momenta in $(T^d)^{\mathbb{Z}_2}$. Moreover, as the rigidity matrices computed by RL satisfy $\tilde{r}(-\mathbf{k}) = g\tilde{r}(\mathbf{k}) = \tilde{r}(\mathbf{k})$ for all $[\mathbf{k}] \in T^d$, an additional avenue would be to classify zero modes in frustrated systems by

$$\pi_0 \left(\left(\Omega^d V_n(\mathbb{C}^m)^{\mathbb{Z}_2} \right)^{\mathbb{Z}_2} \right) \cong \pi_1 \left(\Omega^{d-1} V_n(\mathbb{C}^m)^{\mathbb{Z}_2}, \left(\Omega^{d-1} V_n(\mathbb{C}^m)^{\mathbb{Z}_2} \right)^{\mathbb{Z}_2} \right) \quad (3.15)$$

with the algorithm outlined in equation (A.1). This additionally shows that the homotopy classes in the examples of RL [31] include into our homotopy classes due to the inclusion of the real into the complex Stiefel manifold.

4 Conclusion

In this paper, we proved a generalisation of a result in \mathbb{Z}_2 -equivariant homotopy theory and applied it to frustrated spin systems. The presented applications lead to a homotopical classi-

fication of frustrated systems in the presence or absence of canonical time-reversal symmetry. This homotopical classification of rigidity matrices explains the robust nature of frustration in the form of an accidental degeneracy of ground states in many frustrated magnets by relating it to topological invariants [31]. The zero modes in frustrated magnets are described in the framework of rigidity operators R whose kernels contain the zero modes. The linearized Hamiltonian is given as a bilinear form in terms of R . Moreover, this homotopical classification can also be applied to frustrated n -vector models.

We further demonstrated the emergence of an unstable regime concerning the computation of sets of homotopy classes starting from lattice dimension $d = 3$ for $|\nu| < \lceil d/2 \rceil$, differentiated from the trivial regime $|\nu| \geq \lceil d/2 \rceil$. To complete the topological classification in dimension $d = 3$ and go beyond, one should understand more deeply the topological structure of each path component of $(\Omega^d V_n(\mathbb{C}^m))^{\mathbb{Z}_2}$.

The topological classification is exemplified through the pyrochlore HAF, the HAF on a square lattice with anisotropic next-nearest neighbour interactions and the $J_1 - J_2$ HAF on a square lattice. The results are compared to the ones of RL [31] and it is observed that the homotopy classes in their examples include into our homotopy classes due to the inclusion of the real into the complex Stiefel manifold.

As a next task, one could ask oneself how to calculate

$$\left[(T^d, [\mathbf{0}]), (V_{m-|\nu|}(\mathbb{C}^m), E) \right]_{\mathbb{Z}_2} \quad (4.1)$$

for all $d \geq 1$ to gain access to strong and weak topological invariants. Leaving out the base point preservation condition, one would generalise to the sets of free \mathbb{Z}_2 -homotopy classes [5, p. 96, 17, 13, p. 421]

$$[T^d, V_{m-|\nu|}(\mathbb{C}^m)]_{\mathbb{Z}_2} \cong \left[(T^d, [\mathbf{0}]), (V_{m-|\nu|}(\mathbb{C}^m), E) \right]_{\mathbb{Z}_2} / \pi_1 \left(V_{m-|\nu|}(\mathbb{C}^m)^{\mathbb{Z}_2} \right) \quad (4.2)$$

and

$$[S^d, V_{m-|\nu|}(\mathbb{C}^m)]_{\mathbb{Z}_2} \cong \left[(I^d, \partial I^d), (V_{m-|\nu|}(\mathbb{C}^m), E) \right]_{\mathbb{Z}_2} / \pi_1 \left(V_{m-|\nu|}(\mathbb{C}^m)^{\mathbb{Z}_2} \right) \quad (4.3)$$

for a homotopical classification of time-reversal symmetric frustrated magnets. One could ask further whether there exists a product decomposition of the set $[T^d, V_{m-|\nu|}(\mathbb{C}^m)]_{\mathbb{Z}_2}$ into factors of the already investigated sets of homotopy classes $[(I^d, \partial I^d), (V_{m-|\nu|}(\mathbb{C}^m))]_{\mathbb{Z}_2}$. Or, examine whether there is at least an embedding of the form $[I^d / \partial I^d, V_{m-|\nu|}(\mathbb{C}^m)]_{\mathbb{Z}_2} \hookrightarrow [T^d, V_{m-|\nu|}(\mathbb{C}^m)]_{\mathbb{Z}_2}$. Both of these avenues are true in the context of topological insulators and superconductors (when replacing complex Stiefels manifold with the symmetric spaces in the Bott-Kitaev periodic table) [17].

As a technical generalisation, one shall consider a disjoint union of the form $0 \sqcup \bigsqcup_{p=1}^q V_{n-q+p}(\mathbb{C}^m)$ as target spaces for rigidity matrices. This incorporates rigidity matrices into the classification whose singular values exhibit zeros at certain momenta in the Brillouin torus. Here, $q-1 \in \{0, \dots, n-1\}$ denotes the number of singular values that each have a zero at a certain momentum.

Moreover, one shall investigate more symmetries, e.g. various crystalline symmetries, possibly retrieving \mathbb{Z}_2 -equivariance conditions to realise a homotopical classification through Lemma 3.1.

In three dimensions, there are already 230 crystallographic space group types. In chapter 2.2 we were inspired by the altermagnetic Hubbard model [3] and demonstrated the corresponding rigidity matrix in equation (2.11). One could incorporate the \mathbb{Z}_2 -equivariance condition $\tilde{r}(-\mathbf{k}) = [((-\sigma_1) \oplus (\sigma_1 \otimes \sigma_1)) \oplus (\sigma_1 \oplus (-\sigma_1 \otimes \sigma_1))] \tilde{r}(\mathbf{k}) [\sigma_1 \oplus \sigma_1]$ into the homotopical classification by calculating

$$\pi_0 \left(\left(\Omega^2 V_2(\mathbb{C}^6)^{\mathbb{Z}_2} \right)^{\mathbb{Z}_2} \right), \quad (4.4)$$

where the \mathbb{Z}_2 -action on $V_2(\mathbb{C}^6)$ is a combined \mathbb{Z}_2 -action and either realised by $gA := [(-\sigma_1) \oplus (\sigma_1 \otimes \sigma_1)] \overline{A} \sigma_1$ or by $gA := [\sigma_1 \oplus (-\sigma_1 \otimes \sigma_1)] \overline{A} \sigma_1$. The \mathbb{Z}_2 -action on $\Omega^2 V_2(\mathbb{C}^6)^{\mathbb{Z}_2}$ is realised by $(gf)(\mathbf{k}) = \overline{f(-\mathbf{k})}$.

Finally, as the mean-field Hamiltonian of the altermagnetic Hubbard model [3] is momentum-inversion symmetric, one can employ Lemma 3.1 to obtain a homotopical classification of such Hamiltonians through the algorithm in equation (A.1).

A Main idea to derive Tables 3.1(a) and 3.1(b)

The main idea in computing the sets of \mathbb{Z}_2 -homotopy classes portrayed in Tables 3.1(a) and 3.1(b) is algorithmically portrayed in equation (A.1). The morphisms i_* and j_* are the induced inclusions $i: (\Omega X)^{\mathbb{Z}_2} \hookrightarrow \Omega X$ and $j: (\Omega X, c_{x_0}) \hookrightarrow (\Omega X, (\Omega X)^{\mathbb{Z}_2})$, respectively, and the boundary operator ∂ is defined by evaluating representatives of homotopy classes at $-\pi$.

$$\begin{array}{ccccccc}
& & & & [(I^d, \partial I^d), (X, x_0)]_{\mathbb{Z}_2} & & \\
& & & & \parallel & & \\
\pi_1 \left((\Omega^{d-1} X)^{\mathbb{Z}_2} \right) & \xrightarrow{i_*} & \pi_1(\Omega^{d-1} X) & \xrightarrow{j_*} & \pi_1 \left(\Omega^{d-1} X, (\Omega^{d-1} X)^{\mathbb{Z}_2} \right) & \xrightarrow{\partial} & \pi_0 \left((\Omega^{d-1} X)^{\mathbb{Z}_2} \right) \xrightarrow{i_*} \pi_0(\Omega^{d-1} X) \\
& & \parallel & & \vdots & & \parallel \\
& & \pi_d(X) & & & & \pi_{d-1}(X) \\
& & & & \vdots & & \\
\pi_1 \left((\Omega^2 X)^{\mathbb{Z}_2} \right) & \xrightarrow{i_*} & \pi_1(\Omega^2 X) & \xrightarrow{j_*} & \pi_1 \left(\Omega^2 X, (\Omega^2 X)^{\mathbb{Z}_2} \right) & \xrightarrow{\partial} & \pi_0 \left((\Omega^2 X)^{\mathbb{Z}_2} \right) \xrightarrow{i_*} \pi_0(\Omega^2 X) \\
& \parallel & \parallel & & & & \parallel \\
\pi_2 \left(\Omega X, (\Omega X)^{\mathbb{Z}_2} \right) & & \pi_3(X) & & & & \pi_2(X) \\
& & & & \cong & \nearrow & \\
\pi_1 \left((\Omega X)^{\mathbb{Z}_2} \right) & \xrightarrow{i_*} & \pi_1(\Omega X) & \xrightarrow{j_*} & \pi_1 \left(\Omega X, (\Omega X)^{\mathbb{Z}_2} \right) & \xrightarrow{\partial} & \pi_0 \left((\Omega X)^{\mathbb{Z}_2} \right) \xrightarrow{i_*} \pi_0(\Omega X) \\
& \parallel & \parallel & & & & \parallel \\
\pi_2(X, X^{\mathbb{Z}_2}) & & \pi_2(X) & & & & \pi_1(X) \\
& & & & \cong & \nearrow & \\
\pi_1(X^{\mathbb{Z}_2}) & \xrightarrow{i_*} & \pi_1(X) & \xrightarrow{j_*} & \pi_1(X, X^{\mathbb{Z}_2}) & \xrightarrow{\partial} & \pi_0(X^{\mathbb{Z}_2}) \xrightarrow{i_*} \pi_0(X)
\end{array} \quad (A.1)$$

We stack the ends of the well-known homotopy sequences of based pairs [13, p. 344] of the form $(\Omega^{d-1} X, (\Omega^{d-1} X)^{\mathbb{Z}_2}, c_{x_0})$ for each $d \geq 1$ and connect them via the isomorphisms constructed in Lemma 3.1. We want to calculate the first relative homotopy set in the middle of each exact sequence in equation (A.1). However, the fourth set of homotopy classes in every sequence is another set of path components of a \mathbb{Z}_2 -equivariant iterated loop space in one lattice dimension

less that we are interested in calculating. By Lemma 3.1, this gives rise to a similar exact sequence in one lattice dimension less and the argument iterates. We proceed the iteration until we reach the bottom, i.e., an exact sequence in which the number of loop coordinates has been reduced to 0. In this very sequence we determine every set or group of homotopy classes, in particular the set $\pi_0\left((\Omega X)^{\mathbb{Z}_2}\right) \cong \pi_1(X, X^{\mathbb{Z}_2})$, and move upwards from there by considering the next higher lattice dimension, $d = 2$, and move on.

Acknowledgements

I would like to express my deepest appreciation to my advisor Martin Zirnbauer for guidance and helpful comments. I would like to extend my sincere thanks to Simon Trebst, Krishanu Roychowdhury and Hansjörg Geiges for helpful discussions.

References

- [1] A. Alldridge, C. Max, and M. R. Zirnbauer. Bulk-Boundary Correspondence for Disordered Free-Fermion Topological Phases. *Communications in Mathematical Physics* **377.3** (2019), 1761–1821.
- [2] B. Canals. From the square lattice to the checkerboard lattice: Spin-wave and large- n limit analysis. *Phys. Rev. B* **65.18**, 184408 (2002).
- [3] P. Das et al. *Realizing Altermagnetism in Fermi-Hubbard Models with Ultracold Atoms*. 2023.
- [4] T. tom Dieck. *Algebraic Topology*. EMS textbooks in mathematics. Berlin: European Mathematical Society, 2008.
- [5] T. tom Dieck. *Transformation Groups*. De Gruyter studies in mathematics. Berlin: De Gruyter, 1987.
- [6] T. H. Diep. *Frustrated Spin Systems*. Singapore: World Scientific, 2004.
- [7] M. Dresselhaus, G. Dresselhaus, and A. Jorio. *Group Theory: Application to the Physics of Condensed Matter*. Berlin: Springer-Verlag, 2007.
- [8] F. J. Dyson. Statistical Theory of the Energy Levels of Complex Systems. I. *Journal of Mathematical Physics* **3.1** (2004), 140–156.
- [9] Y. Fang et al. Classification of Classical Spin Liquids: Topological Quantum Chemistry and Crystalline Symmetry. *arXiv: 2309.12652* (2023).
- [10] D. Fiorenza, D. Monaco, and G. Panati. \mathbb{Z}_2 Invariants of Topological Insulators as Geometric Obstructions. *Communications in Mathematical Physics* **343.3** (2016), 1115–1157.
- [11] S. Friedberg, A. Insel, and L. Spence. *Linear Algebra*. Featured Titles for Linear Algebra (Advanced) Series. London: Pearson Education, 2003.
- [12] M. E. Gilmore. Complex Stiefel Manifolds, some homotopy groups and vector fields. *Bulletin of the American Mathematical Society* **73.5** (1967), 630–633.

- [13] A. Hatcher. *Algebraic Topology*. Algebraic Topology. Cambridge: Cambridge University Press, 2002.
- [14] T. L. Hughes, E. Prodan, and B. A. Bernevig. Inversion-symmetric topological insulators. *Phys. Rev. B* **83**.24, 245132 (2011).
- [15] R. M. Kaufmann, D. Li, and B. Wehefritz-Kaufmann. Notes on topological insulators. *Reviews in Mathematical Physics* **28**.10, 1630003 (2016).
- [16] R. Kennedy and M. R. Zirnbauer. Bott–Kitaev periodic table and the diagonal map. *Physica Scripta* **2015**.T164, 014010 (2015).
- [17] R. Kennedy and C. Guggenheim. Homotopy theory of strong and weak topological insulators. *Phys. Rev. B* **91**.24, 245148 (2015).
- [18] R. Kennedy and M. Zirnbauer. Bott Periodicity for \mathbb{Z}_2 Symmetric Ground States of Gapped Free-Fermion Systems. *Communications in Mathematical Physics* **342**.3 (2015), 909–963.
- [19] A. Kitaev. Periodic table for topological insulators and superconductors. *AIP Conference Proceedings* **1134**.1 (2009), 22–30.
- [20] C. Lacroix, P. Mendels, and F. Mila. *Introduction to Frustrated Magnetism: Materials, Experiments, Theory*. Springer Series in Solid-State Sciences. Berlin: Springer-Verlag, 2011.
- [21] E. H. Lieb and P. Schupp. Ground State Properties of a Fully Frustrated Quantum Spin System. *Phys. Rev. Lett.* **83**.25 (1999), 5362–5365.
- [22] A. Ludwig. Topological phases: Classification of topological insulators and superconductors of non-interacting Fermions, and beyond. *Physica Scripta* **2016**.T168, 014001 (2015).
- [23] J. C. Maxwell. L. On the calculation of the equilibrium and stiffness of frames. *The London, Edinburgh, and Dublin Philosophical Magazine and Journal of Science* **27**.182 (1864), 294–299.
- [24] I. Mazin. Editorial: Altermagnetism—A New Punch Line of Fundamental Magnetism. *Phys. Rev. X* **12**.4, 040002 (2022).
- [25] M. Mimura and H. Toda. Homotopy Groups of $SU(3)$, $SU(4)$ and $Sp(2)$. *Journal of Mathematics of Kyoto University* **3**.2 (1963), 217–250.
- [26] R. Moessner and J. T. Chalker. Low-temperature properties of classical geometrically frustrated antiferromagnets. *Physical Review B* **58**.18 (1998), 12049–12062.
- [27] R. Moessner and J. T. Chalker. Properties of a Classical Spin Liquid: The Heisenberg Pyrochlore Antiferromagnet. *Phys. Rev. Lett.* **80**.13 (1998), 2929–2932.
- [28] R. Moessner and A. Ramirez. Geometrical Frustration. *Physics Today* **59**.2 (2006), 24–29.
- [29] M. Nakahara. *Geometry, Topology and Physics, Second Edition*. Graduate student series in physics. London: Taylor & Francis, 2003.
- [30] J. N. Reimers. Absence of long-range order in a three-dimensional geometrically frustrated antiferromagnet. *Phys. Rev. B* **45**.13 (1992), 7287–7294.
- [31] K. Roychowdhury and M. J. Lawler. Classification of magnetic frustration and metamaterials from topology. *Phys. Rev. B* **98**.9, 094432 (2018).

- [32] K. Roychowdhury, D. Z. Rocklin, and M. J. Lawler. Topology and Geometry of Spin Origami. *Physical Review Letters* **121**.17 (2018).
- [33] K. Roychowdhury et al. “Supersymmetry on the lattice: Geometry, Topology, and Spin Liquids”. 2022.
- [34] S. Ryu et al. Topological insulators and superconductors: tenfold way and dimensional hierarchy. *New Journal of Physics* **12**.6, 065010 (2010).
- [35] L. Šmejkal, J. Sinova, and T. Jungwirth. Beyond Conventional Ferromagnetism and Antiferromagnetism: A Phase with Nonrelativistic Spin and Crystal Rotation Symmetry. *Phys. Rev. X* **12**.3, 031042 (2022).
- [36] L. Šmejkal, J. Sinova, and T. Jungwirth. Emerging Research Landscape of Altermagnetism. *Phys. Rev. X* **12**.4, 040501 (2022).
- [37] A. P. Schnyder et al. Classification of Topological Insulators and Superconductors. *AIP Conference Proceedings* **1134**.1 (2009), 10–21.
- [38] A. P. Schnyder et al. Classification of topological insulators and superconductors in three spatial dimensions. *Phys. Rev. B* **78**.19, 195125 (2008).
- [39] Y. Tabata et al. Kagomé Ice State in the Dipolar Spin Ice $\text{Dy}_2\text{Ti}_2\text{O}_7$. *Phys. Rev. Lett.* **97**.25, 257205 (2006).
- [40] G. Thompson. Normal Forms for Skew-Symmetric Matrices and Hamiltonian Systems with First Integrals Linear in Momenta. *Proceedings of the American Mathematical Society* **104**.3 (1988), 910–916.
- [41] A. M. Turner et al. Quantized response and topology of magnetic insulators with inversion symmetry. *Phys. Rev. B* **85**.16, 165120 (2012).
- [42] J. Villain. Spin glass with non-random interactions. *Journal of Physics C: Solid State Physics* **10**.10, 1717 (1977).
- [43] M. A. Xicoténcatl. “On \mathbb{Z}_2 -equivariant loop spaces”. *Recent developments in algebraic topology*. Vol. 407. Contemp. Math. Providence, Rhode Island: American Mathematical Society, 2006, 183–191.
- [44] H. Yan et al. Classification of Classical Spin Liquids: Detailed Formalism and Suite of Examples. *arXiv: 2305.19189* (2023).
- [45] H. Yan et al. Classification of Classical Spin Liquids: Typology and Resulting Landscape. *arXiv: 2305.00155* (2023).